Asian Journal of Pharmaceutical Sciences 14 (2019) 144–153

Available online at www.sciencedirect.com

ScienceDirect

journal homepage: www.elsevier.com/locate/AJPS

Original Research Paper

Synthesis and evaluation of cationic polymeric micelles as carriers of lumbrokinase for targeted thrombolysis

*Yang Pan, Xiahui Wang, Zongning Yin**

Key Laboratory of Drug Targeting and Drug Delivery Systems, West China School of Pharmacy, Sichuan University, Chengdu 610041, China

ARTICLE INFO

Article history:
Received 21 October 2017
Revised 20 December 2017
Accepted 26 March 2018
Available online 16 May 2018

Keywords:
Targeted thrombolysis
Lumbrokinase
Polymeric micelles
ATRP
ROP

ABSTRACT

To achieve targeted thrombolysis, a targeted delivery system of lumbrokinase (LK) was constructed using RGDfk-conjugated hybrid micelles. Based on the specific affinity of RGDfk to glycoprotein complex of GPIIb/IIIa expressed on the surface of membrane of activated platelet, LK loaded targeted micelles (LKTM) can be delivered to thrombus. The hybrid micelles were composed of polycaprolactone-block-poly (2-(dimethylamino) ethyl methacrylate) (PCL-PDMAEMA), methoxy polyethylene glycol-block- polycaprolactone (mPEG-PCL) and RGDfk conjugated polycaprolactone-block- polyethylene glycol (PCL-PEG-RGDfk). PCL-PDMAEMA was synthesized via ring open polymerization (ROP) and atom transfer radical polymerization (ATRP). PCL-PEG-RGDfk was synthesized via ROP and carbodiimide chemistry. The prepared LKTM was characterized by dynamic light scattering (DLS) and transmission electron microscope (TEM). Colloidal stability assay showed the prepared LKTM was stable. Biocompatibility assay was performed to determine the safe concentration range of polymer. The assay of fluorescent distribution *in vivo* demonstrated that LKTM can be efficiently delivered to thrombi *in vivo*. Thrombolysis *in vivo* indicated the thrombolytic potency of LKTM was optimal in all groups. Notably, the laboratory mice treated with LKTM exhibited a significantly shorter tail bleeding time compared to those treated with LK or LK-loaded micelles without RGDfk, which suggested that the targeted delivery of LK using RGDfk-conjugated hybrid micelles effectively reduced the bleeding risk.

* Correspoding author. Key Laboratory of Drug Targeting and Drug Delivery Systems, West China School of Pharmacy, Sichuan University, Chengdu 610041, China.
E-mail address: zongningyin@163.com (Z. Yin).
Peer review under responsibility of Shenyang Pharmaceutical University.

https://doi.org/10.1016/j.ajps.2018.03.004

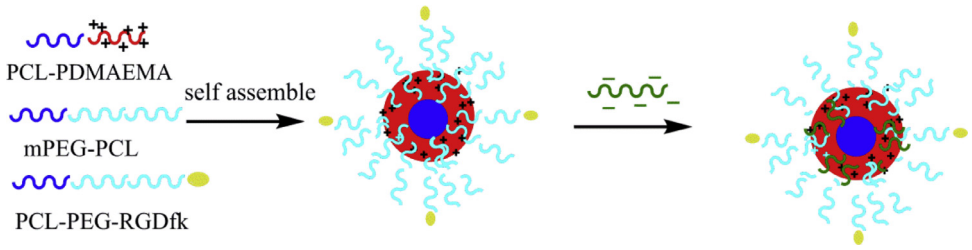

Scheme 1 – The illustration of preparation on LK loaded RGDfk-conjugated mixed micelles.

1. Introduction

Amphiphilic polymer micelles, as excellent nanocarriers, have received tremendous attention in research on drug delivery system (DDS), especial for chemotherapy drug [1], gene [2] and protein [3]. For instance, the amphiphilic polymer constructing the structure of core-shell has been applied in solubilization for hydrophobic drug [4]. The cationic polymers, such as poly (L-lysine) (PLL) [5], polyethyenimine (PEI) [6] polyamidoamine (PAAM) [7], poly (2-(dimethylamino) ethyl methacrylate) (PDMAEMA) [8], have been extensively studied in gene delivery. Compared to nucleic acids and small-molecule drugs, the direct application of protein-based therapies in clinic is limited due to the instability and short shelf-life of protein samples [9]. The lack of suitable carriers for effective delivery to the lesion is another major hurdle for protein-based therapies. In recently studies, protein was mainly delivered by carriers through the electronic interaction [10] or the formation of covalent bond with polymer [11]. Protein-polymer conjugates (PPC) are more stable than protein/polymer complexes formed in electronic interaction *in vivo*, which prone to be used in the controlled release system [12] or improve the stability of protein [12,13]. In addition, protein can be modified to be stimulus-responsive drug through conjugating environment sensitive cross-linker or polymer [14,15]. While protein/polymer complex can be easily formed in a mild condition through electrostatic interaction, it can be easier and more convenient obtained than PPC [16].

Thrombosis, a common cardiovascular disease in clinic, is threatening people's (especially the aged people) health [17]. Fibrinolytic enzyme is necessary for thrombolysis. However, the fibrinogen level would be reduced after the administration of thrombolytic agent, leading to an increase of bleeding risk [18–20] Hemorrhage is a common side effect of fibrinolytic enzyme. In order to reduce the hemorrhagic risk, many studies have been performed to develop targeted delivery of thrombolytic drug to thrombi [21–23]. Notably, platelets play an important role in blood clotting. Prior to clot formation, the platelets become activated upon the formation of the glycoprotein complex GPIIb/IIIa, which is the binding target of Arg-Gly-Asp (RGD)-containing peptides, such as RGDfk [24,25]. Previous reports showed that RGD-conjugated nanoparticles can efficiently bind to GPIIb/IIIa [26–28]. Therefore, we choose RGD-conjugated nanoparticles as the delivery vehicle for fibrinolytic agents in this work so that the fibrinolytic agents can be effectively delivered to thrombus sites.

Cationic polymers have been widely used as the drug delivery carrier for gene and protein drug via electrostatic interaction. Lumbrokinase (LK), a fibrinolytic enzyme originated from earthworm, had been used as the model drug in this work [29]. The isoelectric point of LK is 3–5 [29], allowing for strong electrostatic interactions with cationic polymers under physiological conditions. In our previous study [30], polycaprolactone-block-poly (2-(dimethylamino) ethyl methacrylate)-block poly (2-hydroxyethyl methacrylate) (PCL-PDMAEMA-PHEMA) was used as the carrier of LK. However, the synthesis of PCL-PDMAEMA-PHEMA is challenging, especially for the polymerization of PHEMA block using PCL-PDMAEMA as macroinitiator. The difficult synthesis technology is not easily scaled up and applied in industry. Additionally, methoxy polyethylene glycol-block- polycaprolactone (mPEG-PCL) was used to enhance the colloidal stability and biocompatibility of carriers.

In this work, RGDfk-conjugated mixed micelles were constructed as the carrier of LK for targeted thrombolysis. The preparation procedure of LK-loaded targeted micelles (LKTM) was shown in Scheme 1. We employed PCL-PDMAEMA as the core of our drug delivery carrier. LK can be absorbed to the cationic polymer via electrostatic interactions. In order to covalently link the RGDfk peptide to the carrier, polycaprolactone-block-polyethylene glycol with a carboxylic group (PCL-PEG-COOH) was used as a functionalized polymer. The preparation process of the polymer carrier containing PCL-PDMAEMA, mPEG-PCL and RGDfk-conjugated PCL-PEG-COOH(PCL-PEG-RGDfk) was much simpler than our polymer carrier developed previously [30]. The prepared LKTM was characterized by various spectroscopic techniques and chemical assays to examine its chemical and physical properties. Hemolysis and cytotoxicity assays were performed to determine the safe concentration range of this polymer carrier. *In vivo* thrombolysis assays were performed to assess the fibrinolytic capacity of LKTM. Finally, the tail bleeding assay was taken to evaluate the bleeding risk of LKTM. (Scheme 2).

2. Materials and methods

2.1. Materials

Dodecanol, stannous octoate ($Sn(Oct)_2$), caprolactone, *N, N, N", N", N"'* -Pentamethyldiethylenetriamine (PMDETA), 2-Bromoisobutyryl bromide (2-BiBB), 2-(dimethylamino) ethyl methacrylate (DMAEMA) and cuprous bromide were purchased from Aladdin corporation (Shanghai, China). Cuprous bromide was washed by glacial acetic acid, ethyl

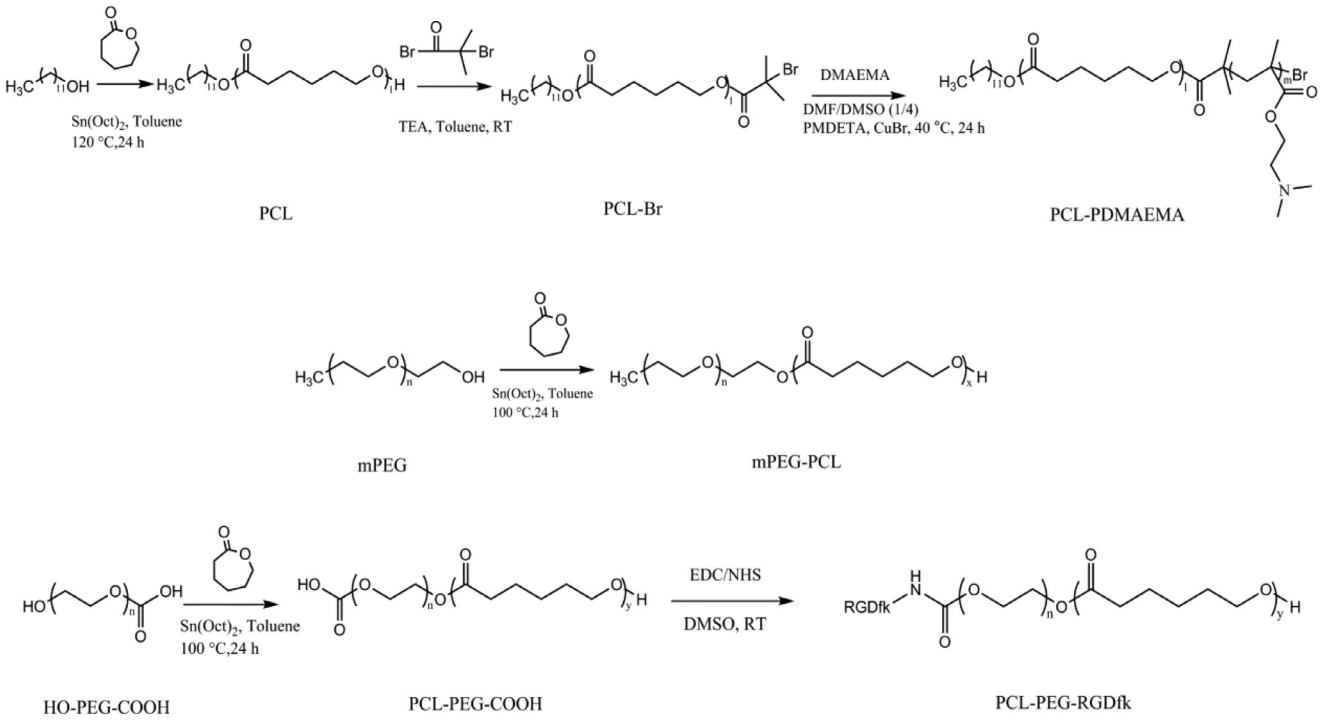

Scheme 2 – Synthetic route of PCL-PDMAEMA, mPEG-PCL and PCL-PEG-RGDfk.

alcohol, and acetone three times for purification. Methoxy polyethylene glycol (mPEG, Mn: 5000 Da) and alpha–hydroxy–omega-carboxy poly (ethylene glycol) (HO-PEG-COOH, Mn: 5000 Da) were purchased from Toyongbio corporation (Shanghai, China). The polymerization inhibitor in DMAEMA was removed by passing an alumina column. 3-(4,5-Dimethylthiazol-2-yl)−2,5-diphenyltetrazolium bromide (MTT) was purchased from Biosharp corporation (Hefei, China). Pyrene was purchased from J&K chemical corporation (Beijing, China). RGDfk (Mw: 603.69) was purchased from Synpeptide Co., Ltd (Shanghai, China). Lumbrokinase (28 000 IU/mg) was obtained from Xi'an Realin Biotechnology Co., Ltd (Xi'an, China). The other agents including *N*, *N*-Dimethylformamide (DMF), dimethylsulfoxide (DMSO), tetrahydrofuran (THF), toluene, triethylamine (TEA), glacial acetic acid, ethyl alcohol, and acetone were obtained from Cdkelongchem corporation (Chengdu, China). Kunming mice and sprague dawley (SD) rats were purchased from Chengdu Dashuo Biological Institute (Chengdu, China). All animal experiments were complied with the guidelines of the Laboratory Protocol of Animal Care and Use Committee, Sichuan University.

2.2. *Synthesis and characterization of PCL-PDMAEMA*

The synthesis and characterization of PCL-PDMAEMA referenced our previous study [30].

2.3. *Synthesis and characterization of mPEG-PCL*

mPEG-PCL was synthesized via ROP using mPEG as the initiator. Briefly, 0.5 g of mPEG (0.1 mmol) was added into a 10 ml schlenk flask and dissolved by 1.0 ml toluene. After addition of 0.456 g of caprolactone (4 mmol) and 76 µl of toluene containing 4 µmol of $Sn(Oct)_2$, the flask was vacuumed and recharged with nitrogen for three times. After heated at 100 °C for 24 h, the reaction mixture was exposed to air to quench the reaction. The toluene in mixture was removed under vacuum in rotary evaporator. The crude product was dissolved in THF and then precipitated in excess cold methanol. The precipitation was isolated and dissolved in THF again. After three times of dissolution/precipitation, the product was dried under vacuum at room temperature. The purified product was characterized by hydrogen nuclear magnetic resonance (^{1}H NMR, 400 MHz, Varian Inc., USA), furier transform infrared spectroscopy (FTIR, PerkinElmer, USA) and gel permeation chromatograph (GPC, Tosoh corporation, Japan).

2.4. *Synthesis and characterization of PCL-PEG-RGDfk*

PCL-PEG-RGDfk was synthesized via two steps. First, PCL-PEG-COOH was synthesized via ROP using HO-PEG-COOH as initiator. The molar ratio of monomer and initiator was 40:1. The protocols of synthesis and characterization were as same as mPEG-PCL. Second, PCL-PEG-RGDfk was synthesized via EDC/NHS chemistry according to the literature [31]. 0.15 g PCL-PEG-COOH (15.69 mmol), 14 mg RGDfk (23.54 mmol), 4.5 mg EDC•HCl (23.54 mmol), 3 mg NHS (23.54 mmol) and 1.5 ml DMSO were added into 10 ml flask. After degassed by three evacuation/nitrogen recharge cycles, the mixture was reacted at room temperature for 24 h. The product was dialyzed (Mn: 2500 Da) against deionized water for 2 d to remove the EDC, NHS and unreacted RGDfk. After lyophilization, the obtained product was characterized by FTIR and ^{1}H NMR.

The content of RGDfk was determined by measuring the arginine content according to the previous report [32].

2.5. Measurement of CMC

Considering the complex polymers were used as carriers, the CMC of mixed micelle of PCL-PDMAEMA and mPEG-PCL was measured using fluorescence spectroscopy. As the content of RGDfk in carriers was low, the RDGfk-conjugated PCL-PEG was not added in this assay. The ratio of PCL-PDMAEMA and mPEG-PCL was 1:1. The concentration of mixed micelles ranged from 0.01–1000 mg/l. The concentration of pyrene stock solution was 6 μM in acetone. The pyrene stock solution (0.3 ml) was added into a 4 ml centrifuge tube. After evaporation of acetone, 3 ml of mixed micelles with different concentration was added, followed by incubation at room temperature for 24 h. The final concentration of pyrene in micelles was 0.6 μM. The excitation spectrum of pyrene was scanned from 300 to 350 nm by using RF5301 PC spectrofluorometer (Shimadzu, Japan) at an emission wavelength of 393 nm. The excitation wavelength at 333 nm shifted to 336 nm with the increasing of concentration of mixed micelles. The CMC value was the concentration of mixed micelles when the ratio of I_{336}/I_{333} was increased with an extreme rate, which determined according to the ratio of I_{336}/I_{333} against to the logarithm of concentration of mixed micelles.

2.6. Preparation of characterization of LKTM

Before the preparation of LKTM, the blank mixed micelles were prepared. Briefly, 10 mg PCL-PDMAEMA, 6 mg mPEG-PCL and 4 mg PCL-PEG-RGDfk were dissolved by 1 ml THF. After addition of 5 ml of deionized water, THF was removed under vacuum by rotary evaporator. The volume of obtained blank mixed micelles was supplemented to 5 ml by deionized water. Next, 0.75 ml of 2.0 mg/ml blank mixed micelles, 0.188 ml of 4.0 mg/ml LK solution and 0.562 ml deionized water were mixed and stirred to form the LK loaded mixed micelles. Considering the instability of LK as protein, the final preparation (LKTM) was prepared as lyophilized powder. 30 mg of manitol and 15 mg of sucrose were added as lyoprotectant in prescription. The hydrodynamic diameter, polydispersity index and zeta potential of LKTM were measured by Zetasizer Nano ZS (Malvern instrument). The morphology of LKTM was characterized by transmission electron microscope (TEM).

2.7. Study on drug loading and release

The free LK in LKTM was isolated via ultrafiltration (300 KDa). The content of free LK was determined by Brandford method. The drug loading content (DLC) and encapsulation efficiency (EE) were calculated according to the content of free LK with the following formulas.

$$\text{DLC (\%)} = \frac{\text{total drug taken} - \text{wt of drug in free}}{\text{wt of micelles}} \times 100\%$$

$$\text{EE (\%)} = \frac{\text{total drug taken} - \text{wt of drug in free}}{\text{total drug of taken}} \times 100\%$$

In vitro release of LK was studied in 0.01 M pH 7.4 PBS at 37 °C. Each sample containing 0.5 ml of LKTM and 4.5 ml releasing medium was set at every sampling time point. 0.4 ml of sample was pipetted to ultracentrifuge tube (Mw: 300 KDa) at every predetermined time point. After centrifugation at 10 000 rpm for 20 min, the released content of LK in filtrate was measured by Brandford method.

2.8. Colloidal stability assay in vitro

The enough colloidal stability is the base for the targeted delivery of therapeutic drug to site of lesion. The colloidal stability of LKTM in PBS containing 10% fetal bovine serum (FBS) was evaluated via the variation of turbidity, particle size and PDI in this study. The increase of turbidity reflects whether there is an aggregate phenomenon of nanoparticles in FBS [33,34]. In turbidity assay, the absorption curve of LKTM diluted 5 times by FBS was scanned by ultraviolet–visible spectrophotometer (Varian Cary 100 Conc, Agilent, U.S.A.) from 400–700 nm to obtain the maximum absorption peak (λ_{max}). Then, the absorbance of LKTM in FBS bathed in water at 37 °C with shaking at 100 rpm was measured at λ_{max} at the preset time point. The sample treated according to the protocol mentioned above was also characterized by dynamic light scattering (DLS) to assess the variation of size and PDI of LKTM.

2.9. Biocompatibility study

2.9.1. Hemolysis assay

The latent hemolytic risk is a commonly problem for kinds of cationic polymers. In order to ensure a good biocompatibility, the concentration cationic polymer should be restricted. According to the literature, the acceptable hemolysis level of drug carriersis10% or lower [35]. In this assay, the concentration of LKTM ranged from 0.1–1.0 mg/ml. After the collection of defibrinated blood from sprague- dawley (SD) mouse, the red blood cell (RBC) was separated by centrifuge at 1200 rpm for 15 min. The isolated RBCs were diluted by PBS to obtain the 2% cell suspension. 100 μl of 2% RBC suspension was mixed with different volume of LKTM (polymer: 2.0 mg/ml). The mixture was supplemented to 200 μl by PBS. After incubation at 37 °C for 1 h, the mixture was centrifuged at 1500 rpm for 5 min. Then 100 μl of supernatant was pipetted to a 96-well plate for the measurement of absorbance at 540 nm by microplate reader. The PBS and 1% triton X-100 treated RBC were used as negative and positive group, respectively.

$$\text{Hemolysis (\%)} = \frac{A_{\text{sample}} - A_{\text{positive}}}{A_{\text{negative}} - A_{\text{positive}}} \times 100\%$$

2.9.2. Cell viability assay

PCL-PDMAEMA, as a cationic polymer, can be absorbed by cell *in vivo* as the cell membrane is a negatively charged surface. The interaction between the cationic polymer and the cell membrane can change the membrane porosity and potential [36]. Cytotoxicity of cationic polymer has been widely studied to evaluate its biocompatibility. It has been shown that mPEG-PCL exhibits an excellent compatibility and low immunogenicity, which has been widely used as drug delivery carriers [37,38]. The low cytotoxicity of mPEG-PCL on L929

cell had been proved in another group [39]. Considering the information mentioned above, we measured the cytotoxicity of PCL-PDMAEMA on L929 cell using MTT assay. The protocol of MTT assay referenced previous report [40]. Briefly, 0.1 ml L929 cells was seeded into a 96-well plate (1.0×10^4 cells per well). After incubation with 5% CO_2 at 37 °C for 24 h, the old cultural medium was renewed by 140 μl fresh Dulbecco's modified Eagle's medium (DMEM) containing 10% fetal bovine serum. Then 60 μl different concentrations of PCL-PDMAEMA in 0.01 M pH 7.4 PBS were added. After incubation for 24 h, 20 μl of 5 mg/ml MTT (in PBS) was added and followed with a cultural for 4 h. Finally, the formazan crystal generated by live cell was dissolved by 200 μl DMSO after removal of the medium. The absorbance was measured at 490 nm using a microplate reader. PBS and 1% triton X-100 treated cell under the same condition were set as the negative and positive control group, respectively. The cell viability was calculated as the follow equation.

$$\text{Cell viability (\%)} = \frac{A_{sample} - A_{positive}}{A_{negative} - A_{positive}} \times 100\%$$

2.10. Study on targeted potential of RGDfk-conjugated mixed micelles in vivo

The targeted potential of RGDfk-conjugated mixed micelles was studied by fluorescent trace technique. mPEG-PCL was labeled by fluorescein isothiocyanate (FITC) using method described previously [41]. The product was characterized by ultraviolet-visible spectrum. LKM (LK-loaded micelles without RGDfk) and LKTM were set as experimental groups. Notably, the LKTM sample used in this set of experiments contained FITC-labeled mPEG-PCL (mPEG-PCL-FITC). In the LKM sample, there was no PCL-PEG-RGDfk; additionally, FITC-labeled mPEG-PCL instead of mPEG-PCL was present. $FeCl_3$-induced carotid artery thrombosis in Kunming mouse (18–22 g) was constructed according to the reported protocol [42]. FITC-containing LKM and LKTM were injected into the mice through the tail vein at a final dosage of 0.012 ml/g (168 U/g). After 2 h of injection, the carotid artery with thrombus in anesthetic mouse was excised for H&E staining. The targeted ability of different materials was compared by the fluorescent distribution.

2.11. Thrombolysis assay in vivo

There were four groups in thrombolysis *in vivo*, including PBS, LK, LKM, LKTM. Five male Kunming mice have been used in each group. After 5 h of formation of thrombus in carotid artery, different materials with the same dose in "2.10″ were injected via tail vein. After 24 h, the carotid artery was excised for H&E staining. The effect of thrombolysis in different groups was evaluated according to the residual thrombi in vessel.

2.12. Determination of bleeding time

Mice-tail bleeding model was used to assess the hemorrhagic risk of thrombolytic agent. The tail of the treated laboratory mouse was transected about 5 mm from the tip. A filter paper was used to touch the incision every 15 s. The bleeding time was determined as the blood no longer blotted into filter in 30 s.

2.13. Statistics

All data in this study were shown as mean ± standard deviation. One-way analysis of variance (ANOVA) was used to determine the statistical significance by SPSS software. In this study, $^*P < 0.05$ and $^{**}P < 0.01$ were used to show statistical significance.

3. Results and discussion

3.1. Synthesis and characterization of mPEG-PCL and PCL-PEG-RGDfk

mPEG-PCL: ^{1}H NMR (400 MHz, $CDCl_3$) δ (ppm): 1.38 (m, $OCOCH_2CH_2\mathbf{CH_2}CH_2CH_2O$ of PCL block), 1.65 (m, $OCOCH_2\mathbf{CH_2}CH_2\mathbf{CH_2}CH_2O$ of PCL block), 2.31 (t, $OCO\mathbf{CH_2}CH_2CH_2CH_2CH_2O$ of PCL block), 3.38(s, $\mathbf{CH_3}O$), 3.64 (m, $O\mathbf{CH_2CH_2}$, $O\mathbf{CH_2}CH_2OCO$ of PEG and $OCOCH_2CH_2CH_2CH_2\mathbf{CH_2}OH$ of PCL), 4.07 (t, $OCOCH_2CH_2CH_2CH_2\mathbf{CH_2}O$ of PCL block), 4.22 (t, $OCH_2\mathbf{CH_2}OCO$).

PCL-PEG-COOH: ^{1}H NMR (400 MHz, DMSO–d_6) δ (ppm): 1.29 (m, $OCOCH_2CH_2\mathbf{CH_2}CH_2CH_2O$ of PCL block), 1.54 (m, $OCOCH_2\mathbf{CH_2}CH_2\mathbf{CH_2}CH_2O$ of PCL block), 2.27 (t, $OCO\mathbf{CH_2}CH_2CH_2CH_2CH_2O$ of PCL block), 3.51 (m, $O\mathbf{CH_2CH_2}$, $O\mathbf{CH_2}CH_2OCO$ of PEG block and $OCOCH_2CH_2CH_2CH_2\mathbf{CH_2}OH$ of PCL), 3.98 (t, $OCOCH_2CH_2CH_2CH_2\mathbf{CH_2}O$ of PCL block), 4.11 (t, $OCH_2\mathbf{CH_2}OCO$ and $HOOC\mathbf{CH_2}OCH_2CH_2$).

PCL-PEG-RGDfk: ^{1}H NMR (400 MHz, DMSO–d_6) δ (ppm): 0.93 (m, R14 of RGDfk), 1.29–1.38 (m, $OCOCH_2CH_2\mathbf{CH_2}CH_2CH_2O$ of PCL block and R10-R12 of RGDfk), 1.55–1.66 (m, $OCOCH_2\mathbf{CH_2}CH_2\mathbf{CH_2}CH_2O$ of PCL block and R13 of RGDfk), 2.27 (t, $OCO\mathbf{CH_2}CH_2CH_2CH_2CH_2O$ of PCL block), 2.65–3.07 (m, R7-R9 of RGDfk), 3.51 (m, $O\mathbf{CH_2CH_2}$, $O\mathbf{CH_2}CH_2OCO$ of PEG block and $OCOCH_2CH_2CH_2CH_2\mathbf{CH_2}OH$ of PCL), 3.98 (t, $OCOCH_2CH_2CH_2CH_2\mathbf{CH_2}O$ of PCL block and R4 of RGDfk), 4.11–4.34 (t, $OCH_2\mathbf{CH_2}OCO$, $HOOC\mathbf{CH_2}OCH_2CH_2$ and R5-R6 of RGDfk), 4.58–4.66 (m, R2-R3 of RGDfk), 7.16–7.22 (m, R1 of RGDfk). As the low content of RGDfk in polymer, the effect of hydrogen in RGDfk on peak shape of hydrogen in PCL-PEG was very poor.

mPEG-PCL and PCL-PEG-COOH were synthesized via ROP using mPEG and HO-PEG-COOH as initiator, respectively. PCL-PEG-RGDfk was synthesized by EDC/NHS chemistry. The ^{1}H NMR and FTIR spectra of synthesized polymer are shown in Fig. S1 and S2. The GPC results of polymers are shown in Table S1 and Fig. S3. As shown in Fig. S1A, the triplet at δ 2.31, 4.07 and multiplet at δ 1.38, 1.65 proved the presence of PCL. The multiplet at δ 3.38 is attributed to the terminal methyl in PEG. Multiplet at δ 3.64 is attributed to the methylene in mPEG and methylene adjacent to hydroxyl in PCL. The signal at δ 4.22 is attributed to the methylene adjoined the PCL block. Its low chemical shift was resulted from the strong electronegativity of ester bond in PCL, which suggested the successful synthesis of mPEG-PCL. The degree of polymerization (DP) of PCL was calculated according to the ratio of peak areas at δ 3.64 and δ

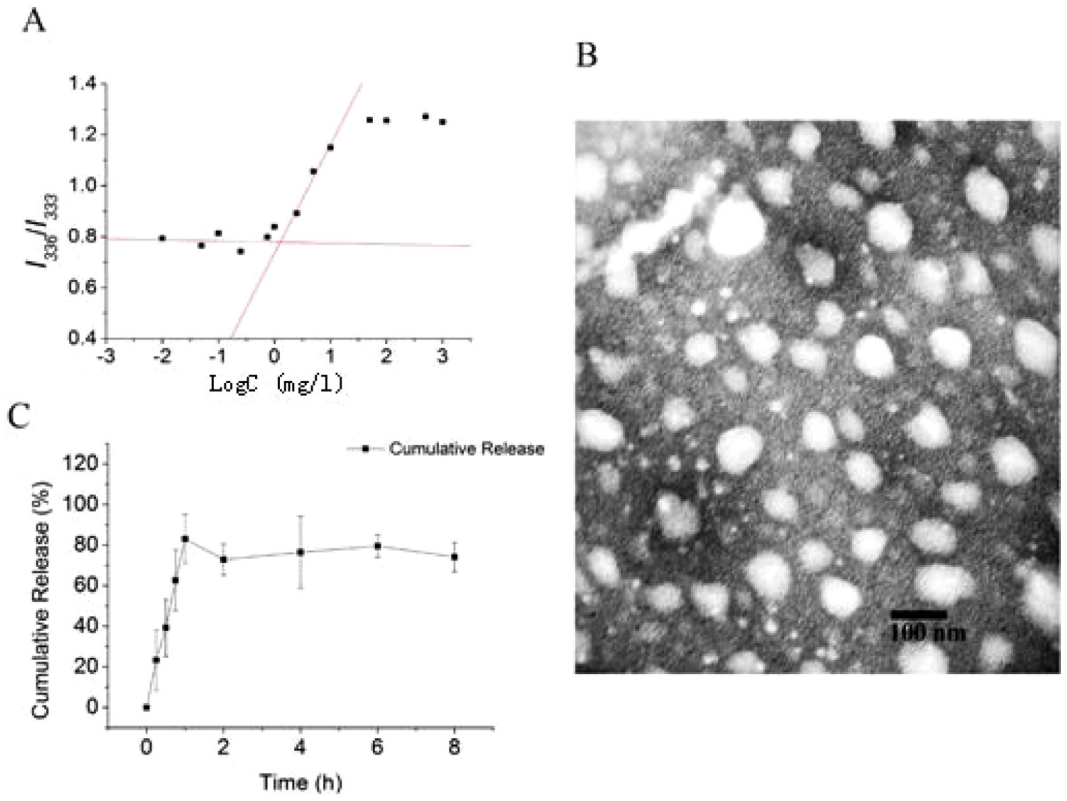

Fig. 1 – (A) Plot of intensity ratio (I_{336}/I_{333}) *versus* logarithm of concentration of mixed micelles. (B) TEM image of LKTM. (C) Percentage of cumulative release of LK from LKTM.

2.31. In ^{1}H NMR spectrum of PCL-PEG-COOH, the analysis of chemical shift was similar to mPEG-PCL. The peaks at δ 1.29, 1.54, 2.27 and 3.98 indicated the presence of PCL block. The DP of PCL was calculated by the ratio of peak areas at δ 3.51 and δ 2.27.

The FT-IR results of the polymers are consistent with the ^{1}H NMR results. After polymerization of ε-caprolactone initiated by mPEG, the extremely strong carbonyl peak from PCL was observed in the FT-IR spectrum, indicating the successful synthesis of mPEG-PCL. A similar result was observed in the IR spectrum of PCL-PEG-COOH.

To confirm the successful conjugation of RGDfk to PCL-PEG-COOH, the ^{1}H NMR spectrum of RGDfk was also characterized. In ^{1}H NMR spectrum of PCL-PEG-RGDfk, the peaks at δ 7.16–7.22, 4.34–4.64, 2.65–3.04, 0.93 proved the presence of RGDfk in polymer. As shown in Fig. S2F, the wavenumbers at 1533 cm^{-1} and 1647 cm^{-1} attributed to benzene ring in RGDfk further supplemented the evidence for the above view. According to the result of determination on the content of arginine, about 55% of PCL-PEG-COOH was labeled by RGDfk. The calibration curve of arginine is shown in Fig. S4.

3.2. *Measurement of CMC*

The CMC value of amphiphilic copolymer closely related to its ability against dilution in blood *in vivo*. A low CMC value (1–5 mg/l) can ensure an enough stability of micelles to avoid the dissociation before arriving the site of lesion [43]. The CMC value of mixed micelles containing PCL-PDMAEMA and mPEG-PCL was 1.27 mg/l according to the intersection point in Fig. 1A. It is evident that the thermodynamic stability of the mixed micelles is excellent.

Table 1 – Results of particle size, PDI, Zeta potential, DLC and EE of LKTM.

Size (nm)	PDI	Zeta potential (mV)	DLC (%)	EE (%)
193.8 ± 0.75	0.176 ± 0.020	38.8 ± 2.42	0.76 ± 0.02	81.59 ± 1.94

3.3. *Characterization of LK loaded mixed micelles*

As shown in Table 1, the particle size, PDI and Zeta potential of LKTM measured by DLS were 193.8 ± 0.75 nm, 0.176 ± 0.020 and 38.8 ± 2.42 mV, respectively. These parameters indicated that the prepared LKTM is composed of uniform and stable nanoparticles. The morphology of LKTM is near spherical as illustrated in the TEM image shown in Fig. 1B.

3.3. *Study on drug loading and release*

The determined values of DLC and EE are shown in Table 1. The EE of mixed micelles was about 80%, which suggested LK can be efficiently absorbed by mixed micelles. The low DLC value was due to the addition of lyoprotectant. The cumulative release curve of LK is shown in Fig. 1C. The rest of LK might be

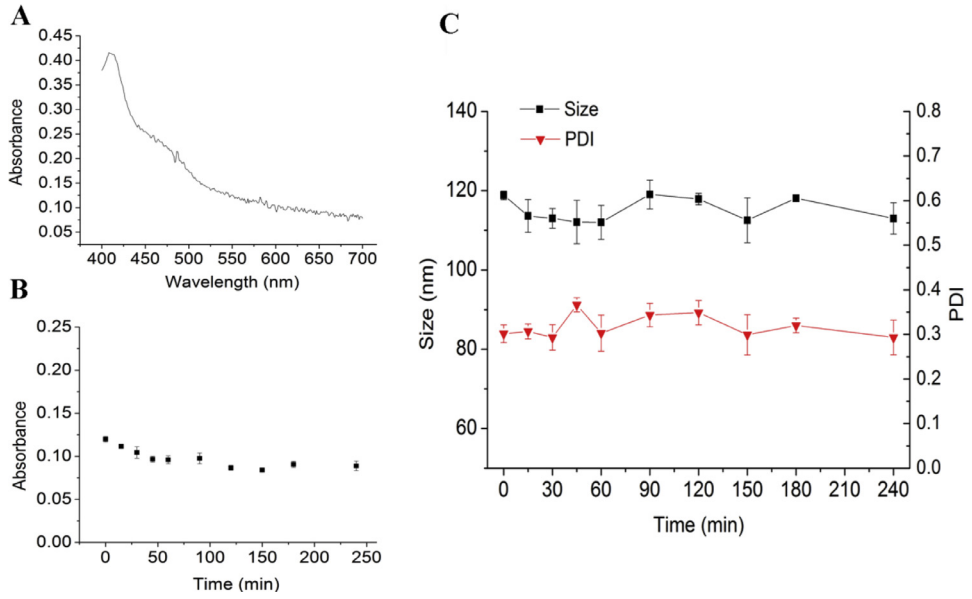

Fig. 2 – Results of colloidal stability assay. (A) UV scanning curve of LKTM, (B) The absorbance of LKTM in 10% FBS, (C) The variation of size and PDI of LKTM in 10% FBS at different time.

ether adsorbed on the surface or loaded into micelles. Meanwhile, it also might be existed in the two type situation mentioned above. The large standard deviation might be resulted from the complexity of protein and the low accuracy of Brandford method.

3.4. *Colloidal stability assay in vitro*

The λ_{max} of LKTM in PBS supplemented with 10% FBS was at 408 nm according to the UV scanning curve. As shown in Fig. 2B, the absorbance of LKTM decreased slightly in 4 h. The slight decrease of absorbance indicated there was no aggregation phenomenon of LKTM in studied medium. The particle size and PDI were keep at about 110–120 nm and 0.30 respectively, which exhibited an excellent stability under the same condition. The few adsorption of FBS might due to the shielding effect of PEG chain. PEG located on the surface of nanoparticles can form a mushroom or hair brush shape structure to impede the adsorption between polymer micelles and FBS. The results above proved the colloidal stability of LKTM in 10% FBS was excellent.

3.5. *Biocompatibility assay*

3.5.1. *Hemolysis assay*

The results of hemolysis assay are shown in Fig. 3A. The hemolysis was lower than 10% when the concentration of polymer was 0.1–0.6 mg/ml. After the concentration of polymer reached at 0.8 mg/ml, the toxicity was unacceptable. Compared with our previous study [31], the biocompatibility of LKTM was significantly better. The improvement might be due to the addition of mPEG-PCL. PEG and its analogues have been widely used to improve the biocompatibility for cationic polymer [36,44]. The results in this work are consistent with previous reports.

3.5.2. *Cell viability assay*

The safe concentration range of PCL-PDAEMA was determined according to the results of cell viability. As shown in Fig. 3B, the viability of PCL-PDMAEMA treated L929 cells was decreased with the increase of concentration. When the concentration of PCL-PDMAEMA was 0.12 mg/ml, the cell viability was lower than 90%. To ensure a good biocompatibility of carriers, the concentration of PCL-PDMAEMA was suggested to no more than 0.09 mg/ml.

3.6. *Study on targeted potential of RGD-conjugated mixed micelles in vivo*

3.6.1. *Characterization of mPEG-PCL-FITC*

The UV–vis spectra of FITC, mPEG-PCL and mPEG-PCL-FITC were collected. As shown in Fig. S5, mPEG-PCL exhibited no absorption in the region of 400–600 nm. FITC displayed absorption peaks at 449 nm and 476 nm. mPEG-PCL-FITC showed similar absorption peaks as those of FITC, indicating that the FITC labeling on mPEG-PCL was successful. The absorption maximum wavelengths of mPEG-PCL-FITC were 459 nm and 487 nm. Compared to the two absorption peaks of free FITC, there was about 10 nm red-shift in both peaks.

3.6.2. *Analysis of fluorescent distribution*

As shown in Fig. 4A and B, both LKTM and LKM induced a decrease in the amount of thrombi in the mice. There were more residual thrombi in the LKM group than the LKTM group, suggesting that LKTM is a better thrombolytic agent. The fluorescent distribution of LKTM and LKM in the carotid artery is shown in Fig. 4C and D, respectively. As shown in Fig. 4C, there is very strong fluorescence in thrombi, indicating that the RGDfk-conjugated polymer can effectively target thrombus. In contrast, there is no florescence in Fig. 4D, suggesting that LKM was not able to specifically target thrombus. Therefore, it can be concluded that the better thrombolytic effect of

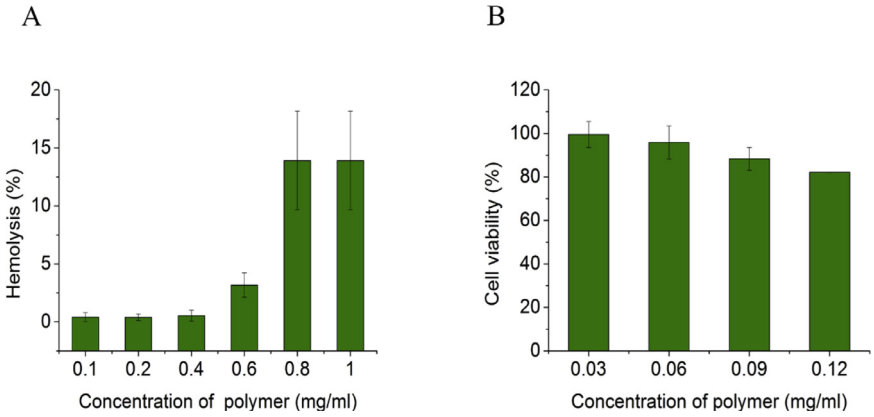

Fig. 3 – (A) Results of hemolysis assay. (B) Results of cell viability in cytotoxicity assay.

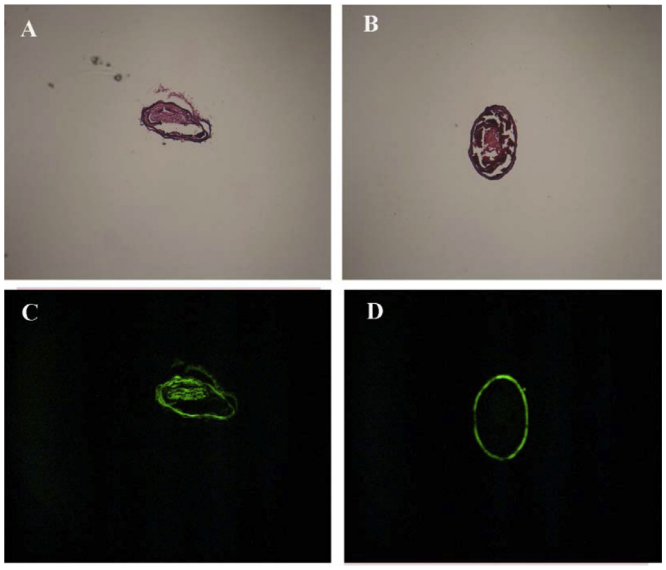

Fig. 4 – Florescent distribution of different experimental groups (magnification 50 × , $n = 5$). (A) LKTM group and (B) LKM group in bright field. (C) LKTM group and (D) LKM group in dark field.

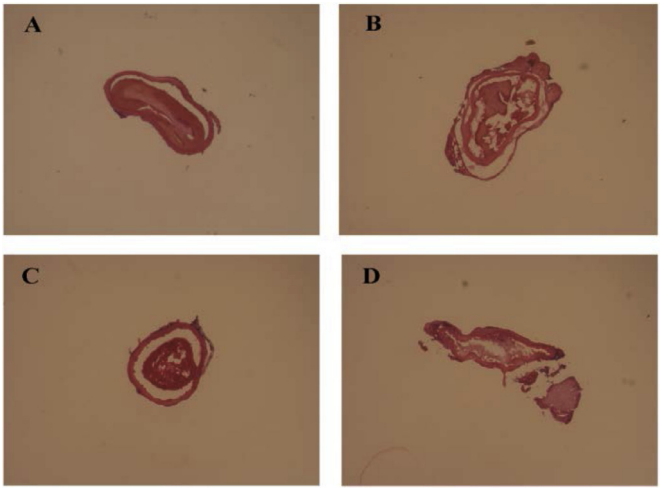

Fig. 5 – The results of thrombolysis in different groups (magnification 100 × , $n = 5$). (A) PBS group, (B) LK group, (C) LKM group, (D) LKTM group.

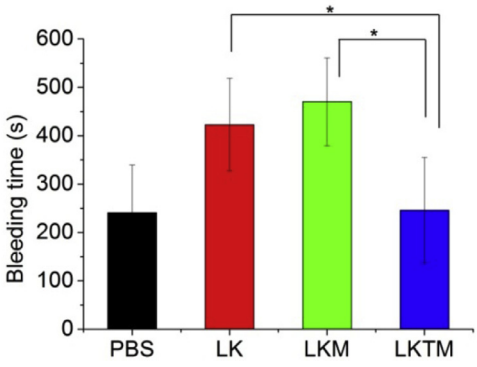

Fig. 6 – Bleeding time of mice in different groups ($n = 4–5$).

LKTM compared to LKM is due to its ability of targeted drug delivery.

3.7. *Thrombolysis assay in vivo*

The different effects of thrombolysis are shown in Fig. 5. PBS group was set as blank control. As shown in Fig. 5A, the thrombi remained unaltered after the administration of PBS. In LK, LKM, LKTM groups, a certain extent thrombolysis proved the efficacy of LK. The rest of clot in LK group was similar with LKM group, which suggested the polymer had little effect on thrombolysis. The LKTM group exhibited the least residual thrombi, which was consistent with the results shown in "3.6". All the results mentioned above proved LK had been successfully delivered to thrombi. The curative effect of LK had been enhanced after targeted delivery using RGDfk-conjugated micelles.

3.8. *Determination of tail bleeding time*

A long tail bleeding time corresponds to a high hemorrhagic risk. As shown in Fig. 6, the bleeding time of LKTM group was significantly shorter than LK and LKM groups ($P = 0.036$ and 0.020, respectively), which indicated the bleeding risk had been reduced due to the targeted drug delivery. The approximate bleeding time in LK group and LKM group ($P = 0.476$) indicated the effect of carriers without RGDfk on bleeding was poor. Thus, RGDfk played a critical role in reducing the bleeding time via the targeted delivery of LK to the lesion sites.

4. Conclusion

In summary, a RGDfk conjugated hybrid micelles for targeted delivery of LK was successfully developed in this work. The particle size of prepared LKTM was homogenous. The colloidal stability and blood compatibility of LKTM were both enhanced than our previous reported LKTM prepared by PCL-PDMAEMA-PHEMA. Fluorescent trace technology *in vivo* proved that LKTM had been successfully delivered to thrombi. Thrombolysis assay *in vivo* suggested the curative effect was improved after the targeted delivery of LK. The results of bleeding time proved the hemorrhagic risk of LK had been reduced, which reached the purpose of this project. Therefore, RGDfk contained cationic polymeric micelles may be as promising candidate for the delivery of LK for targeted thrombolysis.

Conflicts of interest

The authors report no conflicts of interest. The authors alone are responsible for the content and writing of this article.

Acknowledgment

This work was financially supported by National Natural Science Foundation of China (No. 81673363).

Supplementary materials

Supplementary material associated with this article can be found, in the online version, at doi:10.1016/j.ajps.2018.03.004.

REFERENCES

[1] Wang T, Wang D, Yu H, et al. Intracellularly acid-switchable multifunctional micelles for combinational photo/chemotherapy of the drug-resistant tumor. ACS Nano 2016;10(3):3496–508.
[2] Feng G, Chen H, Li J, et al. Gene therapy for nucleus pulposus regeneration by heme oxygenase-1 plasmid DNA carried by mixed polyplex micelles with thermo-responsive heterogeneous coronas. Biomaterials 2015;52:1–13.
[3] Senske M, Smith AE, Pielak GJ. Protein stability in reverse micelles. Angew Chem Int Ed Engl 2016;55(11):3586–9.
[4] Naksuriya O, Shi Y, van Nostrum CF, et al. HPMA-based polymeric micelles for curcumin solubilization and inhibition of cancer cell growth. Eur J Pharm Biopharm 2015;94:501–12.
[5] Kim HJ, Miyata K, Nomoto T, et al. siRNA delivery from triblock copolymer micelles with spatially-ordered compartments of PEG shell, siRNA-loaded intermediate layer, and hydrophobic core. Biomaterials 2014;35(15):4548–56.
[6] Fakhoury JJ, Edwardson TG, Conway JW, et al. Antisense precision polymer micelles require less poly(ethylenimine) for efficient gene knockdown. Nanoscale 2015;7(48):20625–34.
[7] Liu X, Ma D, Tang H, et al. Polyamidoamine dendrimer and oleic acid-functionalized graphene as biocompatible and efficient gene delivery vectors. ACS Appl Mater Interfaces 2014;6(11):8173–83.
[8] Su S, Tian Y, Li Y, et al. "Triple-punch" strategy for triple negative breast cancer therapy with minimized drug dosage and improved antitumor efficacy. ACS Nano 2015;9(2):1367–78.
[9] Osawa S, Osada K, Hiki S, et al. Polyplex Micelles with Double-Protective Compartments of Hydrophilic Shell and Thermoswitchable Palisade of Poly(oxazoline)-Based Block Copolymers for Promoted Gene Transfection. Biomacromolecules 2016;17(1):354–61.
[10] Gao GH, Park MJ, Li Y, et al. The use of pH-sensitive positively charged polymeric micelles for protein delivery. Biomaterials 2012;33(35):9157–64.
[11] Chen W, Shah LA, Yuan L, et al. Polymer–paclitaxel conjugates based on disulfide linkers for controlled drug release. RSC Adv 2015;5(10):7559–66.

[12] Pelegri-O'Day EM, Lin EW, Maynard HD. Therapeutic protein-polymer conjugates: advancing beyond PEGylation. J Am Chem Soc 2014;136(41):14323–32.
[13] Cummings C, Murata H, Koepsel R, Russell A. Dramatically increased pH and temperature stability of chymotrypsin using dual block polymer-based protein engineering. Biomacromolecules 2014;15(3):763–71.
[14] Huang X, Li M, Green DC, et al. Interfacial assembly of protein-polymer nano-conjugates into stimulus-responsive biomimetic protocells. Nat Commun 2013;4:2239.
[15] Jiang Y, Lu H, Chen F, et al. PEGylated albumin-based polyion complex micelles for protein delivery. Biomacromolecules 2016;17(3):808–17.
[16] Bayo-Puxan N, Dufresne MH, Felber AE, Castagner B, Leroux JC. Preparation of polyion complex micelles from poly (ethylene glycol)-block-polyions. J Control Release 2011;156(2):118–27.
[17] Naess IA, Christiansen SC, Romundstad P, et al. Incidence and mortality of venous thrombosis: a population-based study. J Thromb Haemost 2007;5(4):692–9.
[18] Strbian D, Michel P, Seiffge DJ, et al. Symptomatic intracranial hemorrhage after stroke thrombolysis: comparison of prediction scores. Stroke 2014;45(3): 752–758.
[19] Bonnard T, Tennant Z, Niego B, et al. Novel thrombolytic drug based on thrombin cleavable microplasminogen coupled to a single-chain antibody specific for activated GPIIb/IIIa. J Am Heart Assoc 2017;6(2):e004535.
[20] Lee K, Istl A, Dubois L, et al. Fibrinogen level and bleeding risk during catheter-directed thrombolysis using tissue plasminogen activator. Vasc Endovascular Surg 2015;49(7):175–9.
[21] Chen J, Liu C, Hsu H, et al. Magnetically controlled release of recombinant tissue plasminogen activator from chitosan nanocomposites for targeted thrombolysis. J Mater Chem B 2016;4(15):2578–90.
[22] Absar S, Kwon Y M, Ahsan F. Bio-responsive delivery of tissue plasminogen activator for localized thrombolysis. J Control Release 2014;177:42–50.
[23] Bi F, Zhang J, Su Y, Tang YC, Liu JN. Chemical conjugation of urokinase to magnetic nanoparticles for targeted thrombolysis. Biomaterials 2009;30(28):5125–30.
[24] Xie N, Feng K, Chen B, et al. A modular designed copolymer with anti-thrombotic activity and imaging capability. Chem Commun (Camb) 2014;50(67):9539–42.
[25] Saotome T, Hayashi H, Tanaka R, et al. Introduction of VEGF or RGD sequences improves revascularization properties of Bombyx mori silk fibroin produced by transgenic silkworm. J Mater Chem B 2015;3(35):7109–16.
[26] Yang H, Qin C, Yu C, et al. RGD-conjugated nanoscale coordination polymers for targeted T-1- and T-2-weighted magnetic resonance imaging of tumors *in vivo*. Adv Funct Mater 2014;24:1738–47.
[27] Hu H, Arena F, Gianolio E, et al. Mesoporous silica nanoparticles functionalized with fluorescent and MRI reporters for the visualization of murine tumors overexpressing alphavbeta3 receptors. Nanoscale 2016;8(13) 7094-7004.
[28] Fan X, Zhang W, Hu Z, Li Z. Facile synthesis of RGD-conjugated unimolecular micelles based on a polyester dendrimer for targeting drug delivery. J Mater Chem B 2017;5:1062–72.
[29] Nakajima N, Mihara H, Sumi H. Characterization of potent fibrinolytic enzymes in earthworm, Lumbricus rubellus. Biosci Biotechnol Biochem 1993;57(10):1726–30.
[30] Pan Y, Ren X, Wang S, et al. Annexin V-conjugated mixed micelles as a potential drug delivery system for targeted thrombolysis. Biomacromolecules 2017;18(3):865–76.
[31] Diou O, Fattal E, Delplace V, et al. RGD decoration of PEGylated polyester nanocapsules of perfluorooctyl bromide for tumor imaging: influence of pre or post-functionalization on capsule morphology. Eur J Pharm Biopharm 2014;87(1):170–7.
[32] Graf N, Bielenberg DR, Kolishetti N, et al. Alpha(V) beta (3) integrin-targeted PLGA-PEG nanoparticles for enhanced anti-tumor efficacy of a Pt(IV) prodrug. ACS Nano 2012;6(5):4530–9.
[33] Kumar A, Lale SV, Mahajan S, Choudhary V, Koul V. ROP and ATRP fabricated dual targeted redox sensitive polymersomes based on pPEGMA-PCL-ss-PCL-pPEGMA triblock copolymers for breast cancer therapeutics. ACS Appl Mater Interfaces 2015;7(17):9211–27.
[34] Han W, Macewan SR, Chilkoti A, Lopez GP. Bio-inspired synthesis of hybrid silica nanoparticles templated from elastin-like polypeptide micelles. Nanoscale 2015;7(28):12038–44.
[35] Sharma G, Modgil A, Layek B, et al. Cell penetrating peptide tethered bi-ligand liposomes for delivery to brain *in vivo*: Biodistribution and transfection. J Control Release 2013;167(1):1–10.
[36] Venkataraman S, Ong WL, Ong ZY, et al. The role of PEG architecture and molecular weight in the gene transfection performance of PEGylated poly (dimethylaminoethyl methacrylate) based cationic polymers. Biomaterials 2011;32(9):2369–78.
[37] Gao H, Yang Z, Cao S, et al. Tumor cells and neovasculature dual targeting delivery for glioblastoma treatment. Biomaterials 2014;35(7):2374–82.
[38] Deng S, Wu Q, Zhao Y, et al. Biodegradable polymeric micelle-encapsulated doxorubicin suppresses tumor metastasis by killing circulating tumor cells. Nanoscale 2015;7(12):5270–80.
[39] Gong C, Xie Y, Wu Q, et al. Improving anti-tumor activity with polymeric micelles entrapping paclitaxel in pulmonary carcinoma. Nanoscale 2012;4(19):6004–17.
[40] Chen W, Meng F, Cheng R, et al. Facile construction of dual-bioresponsive biodegradable micelles with superior extracellular stability and activated intracellular drug release. J Control Release 2015;210:125–33.
[41] Zhang Z, Qu Q, Li J, Zhou S. The effect of the hydrophilic/hydrophobic ratio of polymeric micelles on their endocytosis pathways into cells. Macromol Biosci 2013;13(6):789–98.
[42] Vu TT, Zhou J, Leslie BA, et al. Arterial thrombosis is accelerated in mice deficient in histidine-rich glycoprotein. Blood 2015;125(17):2712–19.
[43] Xu H, Yao Q, Cai C, et al. Amphiphilic poly (amino acid) based micelles applied to drug delivery: the *in vitro* and *in vivo* challenges and the corresponding potential strategies. J Control Release 2015;199:84–97.
[44] Nelson CE, Kintzing JR, Hanna A, et al. Balancing cationic and hydrophobic content of PEGylated siRNA polyplexes enhances endosome escape, stability, blood circulation time, and bioactivity *in vivo*. ACS Nano 2013;7(10):8870–80.